JMEPEG
https://doi.org/10.1007/s11665-024-09765-0

1059-9495/$19.00

ORIGINAL RESEARCH ARTICLE

Effect of Different Aging Times on the Microstructure and Properties of $Fe_{24}Co_{29}Ni_{38}Al_3Ti_6$ High-Entropy Alloy

Xin Li, Chenglei Wang, Haiqing Qin, Mei Huang, Yatao Zhu, Chong Liu, Hu Chen, Jingya Zhang, and Zhujiang Tan

Submitted: 21 January 2024 / Revised: 5 May 2024 / Accepted: 9 May 2024

$Fe_{24}Co_{29}Ni_{38}Al_3Ti_6$ high-entropy alloy was prepared by vacuum arc melting. Its organization and properties after different aging treatments were investigated. Results show that the high-entropy alloys subjected to different aging treatments are all composed of the FCC matrix phase and the γ' precipitation phase of the $L1_2$ structure with good phase stability. With prolonged aging, the size of the precipitated phase gradually increases, but its volume fraction first increases and then decreases. The wear mechanisms of the high-entropy alloys are abrasive wear and oxidative wear. When the aging time is more than 16 h, the high-entropy alloys show exfoliation wear. When the aging time is 16 h, the precipitation phase of the alloy is uniformly distributed and the volume fraction is the highest. At this time, the alloy has the most excellent wear resistance and tensile properties. The tensile strength, yield strength, and elongation are ~ 1275, 1117 MPa, and ~ 25.2%, respectively. The fracture mechanism is ductile fracture. Aging treatment for different times has a certain effect on the mechanical properties of the alloy and allows the alloy to precipitate precipitated phases with different volume fractions.

Keywords hardness, high-entropy alloys, microstructure, tensile properties, wear resistance

1. Introduction

With the rapid development of science and technology and industry, human beings impose increasingly high requirements for material performance. Especially in the field of mechanical engineering, the problem of material failure due to wear and tear has become prominent, and the wear and tear of materials cause huge economic losses every year. Therefore, alloys with good wear resistance must be further developed to minimize the problem of material wear failure and to save resources. Conventional alloys, such as titanium alloys and stainless steel, are commonly used with one or two metal elements as the primary element. Small amounts of other elements are added to enhance the properties of the alloy. However, when added with too many types of minor elements, the alloy might produce complex brittle phases and intermetallic compounds, which weaken its overall performance. The minor elements in traditional alloys cannot be added at will, greatly limiting the development of traditional alloys. Owing to the continuous development of modern manufacturing industry, traditional alloys are gradually failing to meet the increasing performance requirements of metal materials. At this time, high-entropy alloys (HEAs) came into being. HEAs are a new class of alloys developed by Yeh et al. (Ref 1, 2) using a mixture of multiple elements in similar atomic proportions. They consist of 5-13 elements, each with atomic percentage between 5 and 35%. HEAs possess better properties than conventional metallic materials, such as high strength (Ref 3), friction resistance (Ref 4), corrosion resistance (Ref 5), and resistance to high-temperature oxidation (Ref 6). Although HEAs have multiple components, their structure leads to great mutual solubility between its constituent elements. As a consequence, the generation of intermetallic compounds is avoided and the formation of structurally simple solid solutions is preferred (Ref 7-9). Compared with conventional alloys, HEAs rely on their multicomponent intrinsic structure, which is chemically disordered and capable of inducing severe lattice distortions, retarded element diffusion, and complex stress fields at the atomic level (Ref 10-12). These unique advantages render HEAs with a broad development prospect in new material applications.

HEAs have attracted attention from researchers since their introduction. Numerous studies have shown that HEAs have excellent wear resistance. Liu et al. (Ref 13) investigated the effect of different B contents on the wear properties of $Al_{0.5}CoCrCuFeNiB_x$ HEA and found that the wear resistance of the alloy increases with the B content when $x \geq 0.4$. Nguyen et al. (Ref 14) investigated the high-temperature frictional wear properties of $CrFeNiAl_{0.4}Ti_{0.2}$ HEA and discovered that at 800 °C, the alloy has the lowest wear rate and good wear resistance. Xiao et al. (Ref 15) studied the effect of different sintering processes on the organization and properties of $FeAlCoCrNiTi_{0.5}$ HEA and found that the alloy exhibits dense organization and good grain refinement when the sintering

Xin Li, Chenglei Wang, Mei Huang, Yatao Zhu, Chong Liu, Hu Chen, Jingya Zhang, and **Zhujiang Tan**, School of Materials Science and Engineering, Guangxi Key Laboratory of Information Materials, Engineering Research Center of Electronic Information Materials and Devices, Ministry of Education, Guilin University of Electronic Technology, Guilin 541004, People's Republic of China; and **Haiqing Qin**, Guangxi Key Laboratory of Superhard Material, National Engineering Research Center for Special Mineral Material, China Nonferrous Metal (Guilin) Geology and Mining Co., Ltd., Guilin 541004 Guangxi, People's Republic of China. Contact e-mails: clw0919@163.com and qinhaiqing5218@163.com.

Published online: 05 July 2024

temperature is 1000 °C and the holding time is 3 h. In addition, the alloy has excellent hardness and friction and wear properties. Therefore, HEAs have a certain potential as wear-resistant materials.

FeCoNiAlTi HEAs have been favored by researchers due to their significant advantages in terms of high strength and high plasticity. Vickey et al. (Ref 16) investigated the effect of aging temperature on $Al_{0.2}Co_{1.5}CrFeNi_{1.5}Ti_{0.3}$ HEA and found that when the aging temperature is 750 °C and the aging time is 200 h, the density and size of the precipitated phase are large and the alloy shows the highest hardness. Lu et al. (Ref 17) investigated the effect of aging temperature on the mechanical properties of $Al_{0.3}CoCrFeNiTi_{0.15}$ HEA and discovered that the alloy has the highest ultimate tensile strength (769 MPa) and large elongation at break (32.5%) at 700 °C. Peng et al. (Ref 18) reported the effect of aging treatment on the mechanical properties of $Ni_{28}Co_{28}Fe_{21}Cr_{15}Al_4Ti_4$ HEA. The tensile properties of the alloy peaks after aging treatment at 800 °C for 24 h, with the yield strength reaching 855 MPa and the ultimate tensile strength reaching 1031 MPa. Research on FeCoNiAlTi HEAs mainly focuses on the effect of aging treatment on their phase structure and mechanical properties. However, systematic investigations on the tribological behavior of FeCoNiAlTi HEAs are lacking.

On the basis of the current research status of HEAs and the previous exploration experience, $Fe_{24}Co_{29}Ni_{38}Al_3Ti_6$ HEA was selected as the research object in the present study. The effects of different aging times on the organization and structure evolution, wear behavior, and mechanical properties of $Fe_{24}Co_{29}Ni_{38}Al_3Ti_6$ HEA were explored by subjecting the alloy to different aging treatments. This work aimed to provide experimental and theoretical basis for the development of HEAs with excellent properties.

2. Experimental

$Fe_{24}Co_{29}Ni_{38}Al_3Ti_6$ HEA was prepared by vacuum arc melting under high-purity argon gas protection. The raw materials used were Fe, Co, Ni, Al, and Ti metal monomers with purity higher than 99.95 wt.%. All the raw materials were ultrasonically cleaned to remove impurities before weighing and batching. Melting was repeated more than five times to ensure uniform alloy composition. The weight of a single ingot of HEA obtained by melting is about 29.8 g. The alloy ingots were homogenized at 1200 °C for 8 hours and water quenched. The alloy was then cold rolled at 70% by volume. The cold rolled sheets were recrystallized at 1200 °C for 2 minutes to remove the internal stresses generated within the cold rolled sheets and then aged at 800 °C for different times (4, 8, 16, 32, 64, and 128 h).

The hardness of the alloys was tested using a HV-1000 micro Vickers hardness tester. The load was 1 kg, and the holding time was 15 s. Ten different positions were selected for each alloy to ensure the accuracy of the results. The wear resistance of the alloys was tested using an HSR-2 M high-speed reciprocating friction and wear tester. The abrasive material was Si_3N_4 ball with a diameter of 3 mm, the loading load was 10 N, the running time was 30 min, the reciprocating distance was 5 mm, the rotational speed was 300 rpm, and the sampling frequency was 30 Hz. Five reciprocating friction and abrasion tests were carried out for each alloy under the same conditions to ensure the reproducibility of the tests. The tensile properties of the alloys were tested using an AGX-50kNVD electronic universal testing machine at room temperature. The strain rate was 0.2 mm/min. The alloy specimens used for tensile testing were all approximately 35 mm long, 10 mm wide and 2 mm thick, with a 10-mm scale length. The physical phase of the alloys was analyzed using a Bruker D8 Advance type x-ray diffractometer (XRD) with a scanning range of 20-100° and a scanning step of 7°/min. The microstructure, wear morphology, and tensile fracture morphology of the alloys were analyzed using a Quanta FEG 450 scanning electron microscope (SEM) equipped with an x-ray spectrum analyzer (EDS).

3. Results and Discussion

3.1 Phase Composition and Microstructure Analysis

Figure 1 shows the XRD patterns of $Fe_{24}Co_{29}Ni_{38}Al_3Ti_6$ HEAs after different aging treatments analyzed using the physical phase search software MDI Jade 6. All the alloys consist of a simple FCC solid solution with an $L1_2$ structural intermetallic compound (γ' precipitation phase) composed of Ni_3(Ti, Al). No complex intermetallic compound phases were detected in the XRD accuracy range due to the high mixing entropy effect of HEAs, resulting in the mixing entropy of the system being greater than that for the formation of intermetallic compounds. This phenomenon inhibits the formation of complex intermetallic compounds and promotes mixing between elements to form simple BCC or FCC structures (Ref 19, 20). Owing to their very slow diffusion rate, the elements in the HEA are difficult to precipitate during the aging treatment (Ref 21, 22). As a consequence, a simple solid solution structure is formed.

Figure 2 shows the SEM images of $Fe_{24}Co_{29}Ni_{38}Al_3Ti_6$ HEAs after different aging treatments and their localized enlargements. As illustrated in the macroscopic diagram, the grain distribution of the HEAs is uniform, and the grain size increases gradually with prolonged aging. As displayed in the localized enlargement, all the HEAs precipitate bright $L1_2$ precipitated phases (γ' precipitated phases) on the dark FCC

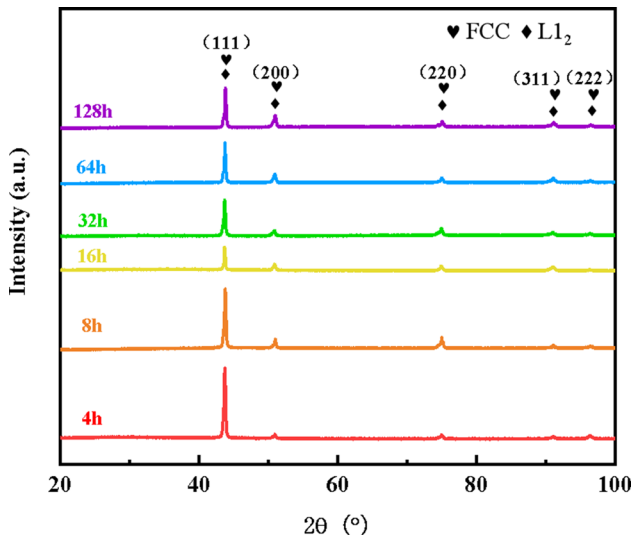

Fig. 1 XRD patterns of HEAs after different aging treatments

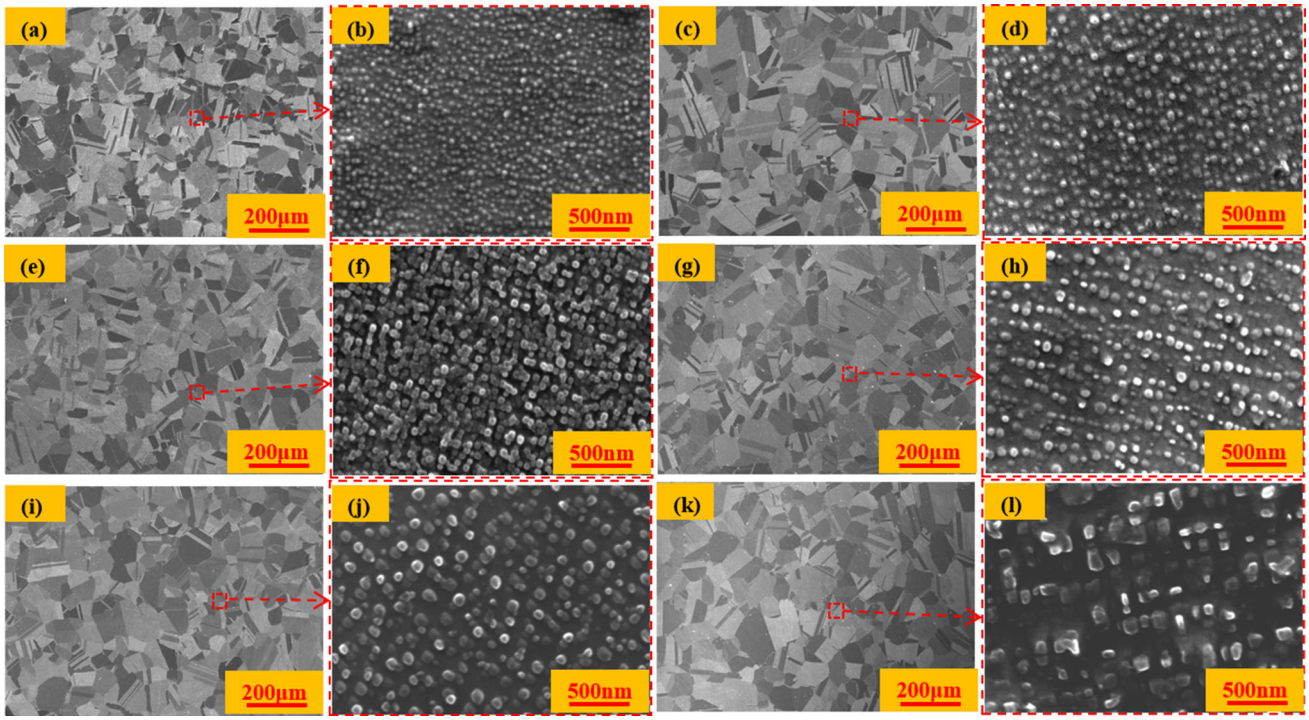

Fig. 2 SEM images of HEAs after different aging treatments: (a) 4 h, (c) 8 h, (e) 16 h, (g) 32 h, (i) 64 h, (k) 128 h; (b), (d), (f), (h), (j), and (l) are the localized enlarged images of the corresponding regions, respectively

matrix. The alloys all have a pronounced "$\gamma' + \gamma$" duplex structure, which is consistent with the XRD analytical results and some previous reports (Ref 23, 24). The $L1_2$ precipitated phase has a size of 30-120 nm and is uniformly dispersed on the FCC substrate.

The volume fraction of $L1_2$ precipitated phase in the alloy does not increase with aging time. Rather, it shows a tendency to first increase and then decrease with prolonged aging. When the aging time is less than 16 h, the precipitated phase is gradually coarsens with the extension of aging time and precipitates out from the matrix. When the aging time is 16 h, the precipitated phase in the HEA completely precipitates from the matrix and reaches the maximum volume fraction. When the aging time is more than 16 h, the precipitated phase gradually dissolves into the matrix and its volume fraction gradually decreases with the extension of aging time. When the matrix is oversaturated, the alloy precipitates fine precipitated phase again and secondary precipitation occurs. When the aging time is 128 h, the morphology of the precipitated phase changes from the previous ellipsoidal morphology to irregular morphology.

3.2 Hardness and Wear Resistance Analysis

Figure 3 shows the hardness and friction and wear properties of HEAs after different aging treatments: (a) coefficient of friction, (b) wear cross section, (c) amount of wear, and (d) average coefficient of friction and hardness. In Fig. 3(a), the friction coefficients of the alloys after different aging treatments possess the same pattern. The friction coefficient curves of the alloys all fluctuate with a large magnitude in the initial stage and flatten out in the later stages. At the initial stage of friction, the surface of the alloy is relatively smooth with low roughness and frictional resistance, resulting in a low friction coefficient. With the increase in the friction time, the contact surface of the alloy and Si_3N_4 on the grinding ball produces a violent adhesion effect, resulting in a rapid increase in the friction coefficient. After a short break-in phase, the wear process enters the stabilization period. The friction coefficient tends to stabilize, entering the stable wear phase. As shown in Fig. 3(b), (c), the HEA after 16 h of aging has the shallowest depth of abrasion marks and the lowest amount of wear. Figure 3(d) shows that the average alloy friction coefficient is negatively correlated with the alloy hardness. The friction coefficient of a material is an important parameter used to characterize its wear resistance. The higher the average friction coefficient, the lower the hardness, and the poorer the wear properties of the alloy (Ref 25, 26). The HEA after 16 h of aging has the lowest average friction coefficient and the highest hardness, indicating that it has the best wear resistance.

The wear morphology of all HEAs was analyzed using SEM and EDS to further investigate the wear behavior of the alloys. Figure 4 and 5 show the surface morphology of all the alloys after reciprocal friction wear and the distribution of surface elemental content after friction wear, respectively. As displayed in Fig. 4, the surface of the alloy wear marks after different aging treatments are distributed with a large number of parallel plow furrows, piled up abrasive chips, or scattered fragments. Material spalling is observed on the wear surfaces of the HEAs subjected to aging for 32, 64, and 128 h. Figure 5 reveals a

large amount of O present on the wear surface of the alloys after different aging treatments. During the friction process, all alloys undergo oxidation on their wear surfaces, forming oxide films. The oxide film generated by alloys during friction can play a lubricating role (Ref 27, 28). It also hinders the direct contact between the surface of the alloy and the friction vice, effectively slowing down the wear of the material and consequently improving the wear resistance of the alloy. The wear surface of the HEA subjected to 16 h of aging has the most uniform O distribution, and its oxide layer covers a large and relatively continuous area. When aged for 16 h, the HEA precipitates a large number of diffusely distributed $L1_2$ precipitation phase, leading to the abrasion of the uniform force and delaying the spalling of the alloy wear surface. With prolonged aging, the particle size of the precipitated phase gradually increases and volume expansion possibly occurs in the wear process. Local stress becomes concentrated, thus producing cracks and spalling. The continuous coarsening of the precipitated phase leads to a reduction of the phase interface, and when the critical shear stress required for dislocations to bypass the precipitated phase is lower than that required to cut through the precipitated phase, the hindering effect of the precipitated phase on the dislocations shifts from a cut-through mechanism to an Orowan bypass mechanism, which leads to a deterioration of the wear resistance of the alloy (Ref 29, 30). In summary, abrasive wear and oxidative wear occur in all the alloys, and spalling wear occurs in the HEAs aged for 32, 64, and 128 h.

3.3 Tensile Properties Analysis

Figure 6 shows the tensile properties of HEAs at room temperature after different aging treatments: (a) tensile curves, (b) comparison of alloy properties, (c) tensile and yield strengths, and (d) elongation. The HEA subjected to 16 h of aging has the highest tensile strength, yield strength, and elongation of ~ 1275 MPa, ~ 1117 MPa, and ~ 25.2%, respectively. The tensile strength and elongation at break of this HEA are higher than those of conventional alloys that are widely used today. It also has excellent tensile properties and

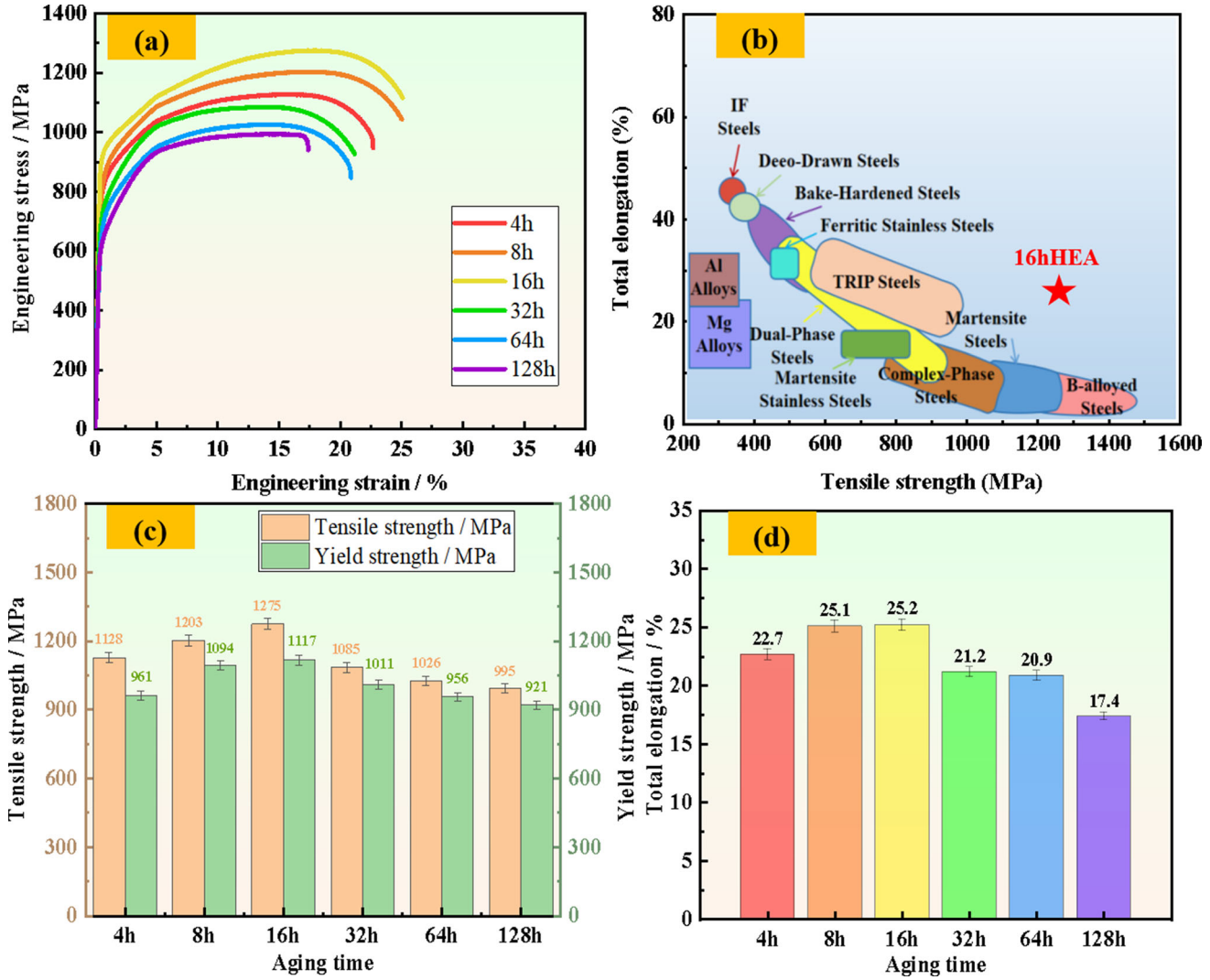

Fig. 3 Hardness and wear resistance of HEAs after different aging treatments: (a) coefficient of friction, (b) wear cross section, (c) amount of wear, (d) average coefficient of friction and hardness

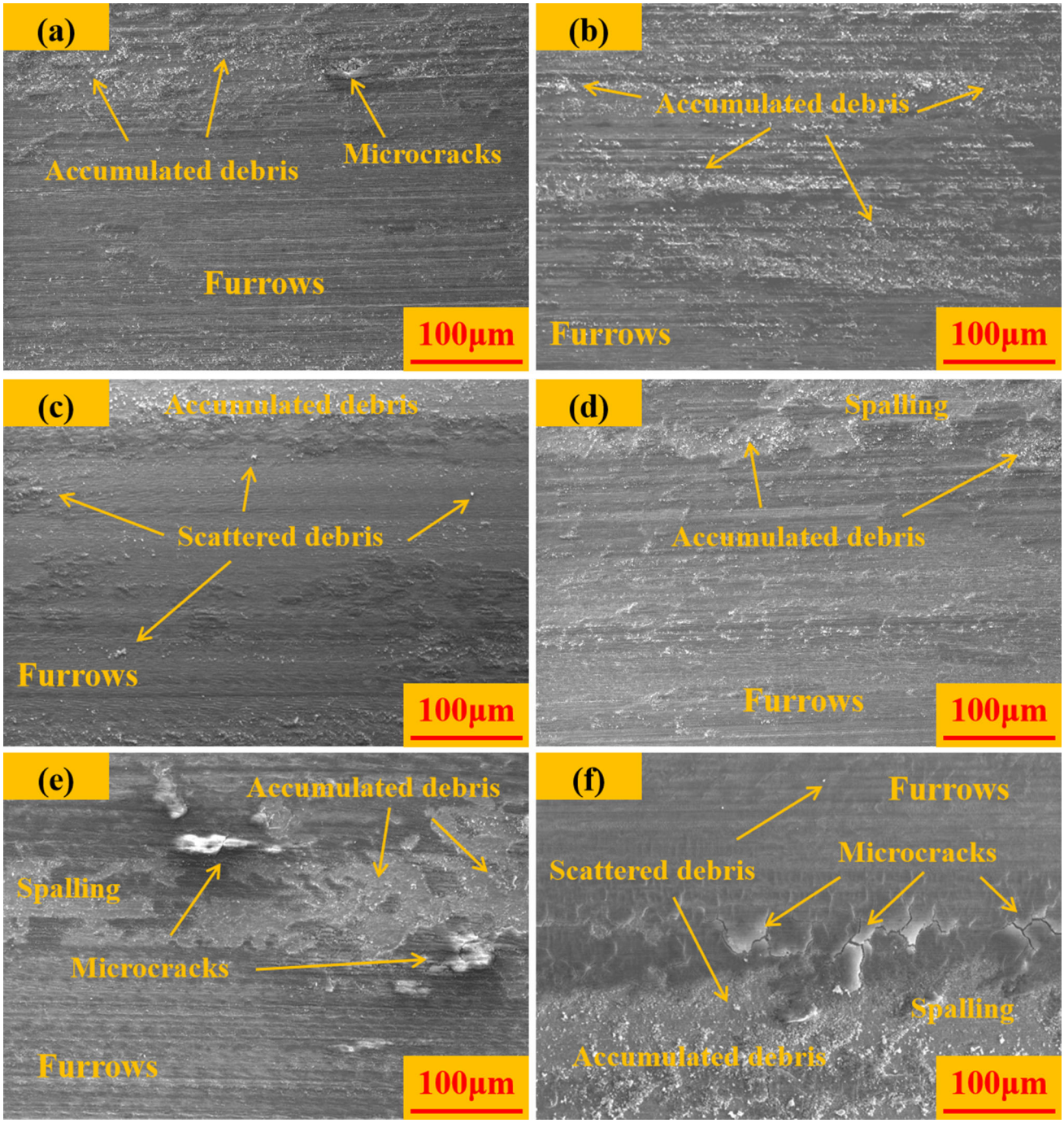

Fig. 4 Surface morphology of HEAs after reciprocating frictional wear: (a) 4 h, (b) 8 h, (c) 16 h, (d) 32 h, (e) 64 h, (f) 128 h.

shows great potential in the engineering and application of structural materials.

The fracture morphology of an alloy after tensile fracture can also reflect its tensile properties (Ref 31). Therefore, the fracture mechanism of the alloys was further explored by analyzing its tensile fracture morphology. Its localized map is shown in Fig. 7. Many tough nests are distributed on the fracture surface of HEAs after different aging treatments, which is a typical characteristic of toughness fracture. When the aging time is 128 h, many cracks distributed along the grain boundaries have appeared on the fracture surface of the HEA. Crystal fracture also occurs. Toughness fracture occurs in

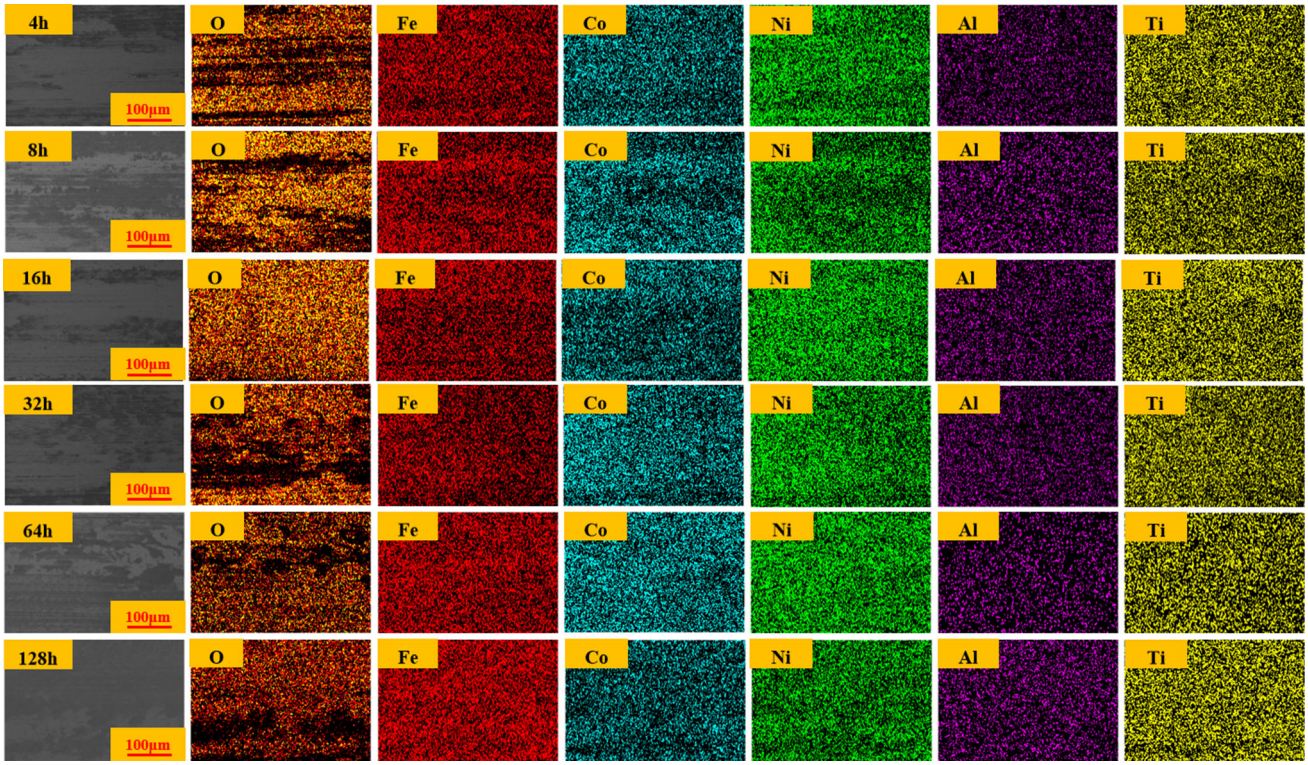

Fig. 5 EDS surface scan of the wear morphology of the alloy surface

metals through the growth and aggregation of micropores. Tough nests are an essential feature of fracture by micropore aggregation. The size of the ligamentous fossa at the fracture of the alloy shows a tendency to increase and then decrease with the extension of the aging time. The larger the size of the ligamentous fossa, the higher the plasticity of the alloy (Ref 32, 33). The HEA with aging time of 16 h has the largest tough nests and highest elongation, which are in agreement with the results of the tensile experiments. The HEA with aging time of 16 h exhibits good tensile and yield strengths while maintaining its own good plasticity because the second phase strengthening plays a dominant role when the $L1_2$ phase is present in the alloy. In addition, the HEA with aging time of 16 h has the highest average volume fraction of precipitated phases, resulting in a high strength. The $L1_2$ precipitated phase in HEAs can maintain a high degree of co-lattice relationship with the FCC matrix phase, which can improve the strength of HEAs while still maintaining good plasticity. When the precipitated phase is small or the volume fraction is high, it will lead to the increase in dislocation resistance, which will greatly improve the properties of the alloy. When the size of the precipitated phase in the alloy is large, the mechanism of dislocation crossing the precipitated phase changes from a cut-through mechanism to an Orowan bypass mechanism, which leads to the deterioration of the alloy's properties (Ref 34, 35). The strength of this alloy has a good positive correlation with its hardness. Hardness is a key indicator of the wear resistance of an alloy; the higher the hardness of the alloy, the better its wear resistance (Ref 36). Hence, the HEA with aging time of 16 h has excellent wear resistance, high plasticity, high strength, and high hardness, which are consistent with the results of the previous experiments.

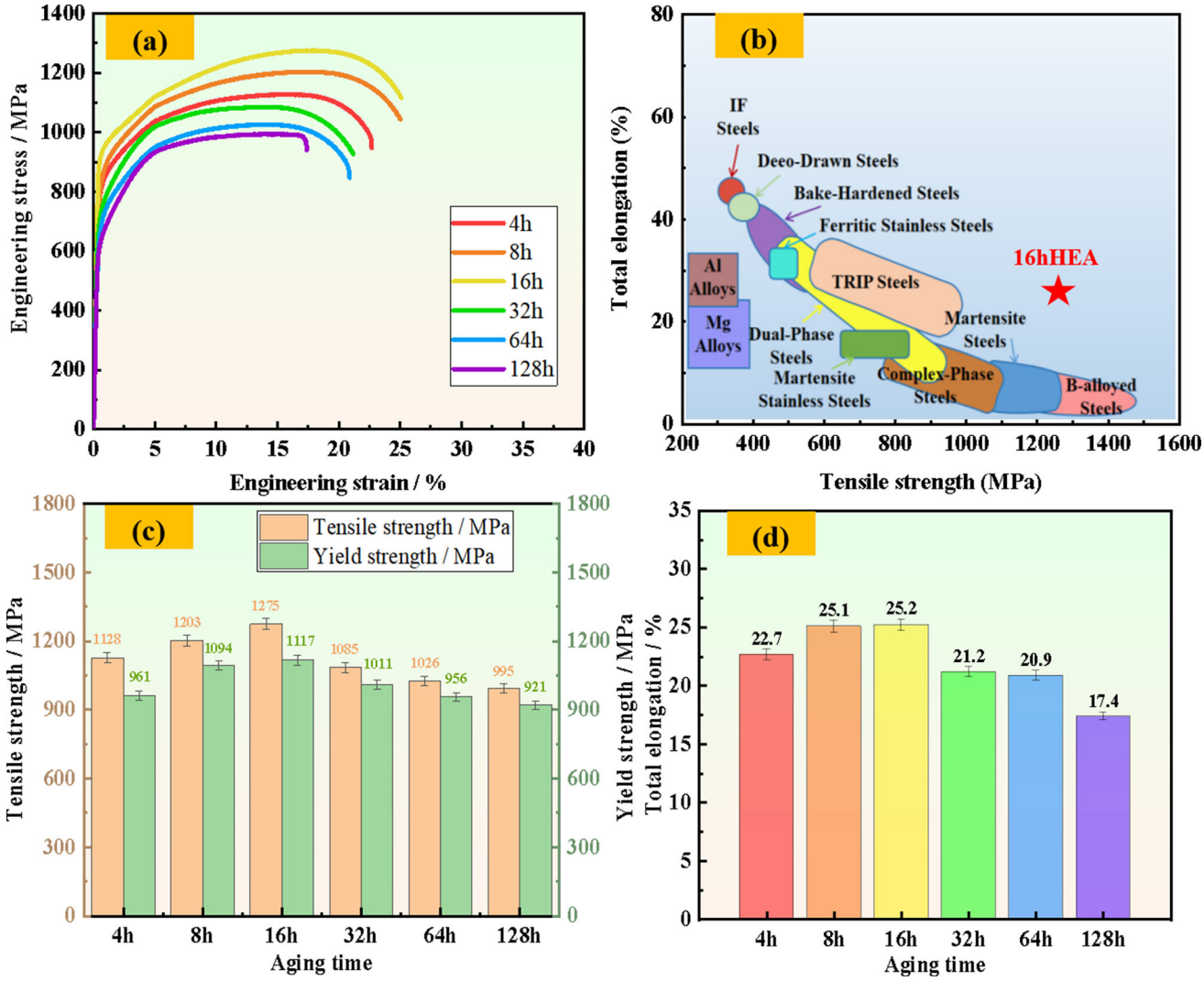

Fig. 6 The tensile properties of HEAs at room temperature after different aging treatments: (a) tensile curves, (b) comparison of alloy properties, (c) tensile and yield strengths, and (d) elongation

4. Summary and Conclusions

$Fe_{24}Co_{29}Ni_{38}Al_3Ti_6$ HEAs were prepared by vacuum arc melting and subjected to different aging heat treatments. The microstructure, microstructure organization, hardness, wear resistance, and tensile properties of the HEAs were also analyzed using XRD, SEM/EDS, microhardness tester, friction and wear tester, and tensile tester. The following results were obtained:

(1) After treatment with different aging times at 800 °C, the $Fe_{24}Co_{29}Ni_{38}Al_3Ti_6$ HEAs are able to maintain their "$\gamma' + \gamma$" dual-phase structure without forming complex intermetallic compounds.
(2) With prolonged aging, the precipitated phase of $L1_2$ gradually coarsens, and its average volume fraction increases and then decreases. When the aging time is 16 h, the precipitated phase of the alloy has the highest average volume fraction. When the aging time exceeds 16 h, the alloy gradually precipitates the second phase particles again.
(3) When the aging time is 16 h, the alloy has the shallowest wear marks, lowest wear amount, lowest average friction coefficient, and highest hardness. Its wear resistance is relatively good. The wear mechanisms of the alloys after different aging treatments include abrasive wear and oxidative wear. When the aging time exceeds 16 h, the wear mechanism of the alloys also includes spalling wear.
(4) The alloy with aging time of 16 h has the highest tensile strength, yield strength, and elongation of ~ 1275 MPa, 1117 MPa, and ~ 25.2 %, respectively. Its tensile properties are generally higher than those of conventional alloys. All the alloys exhibit ductile fracture as the fracture mechanism, except for the HEA with aging time of 128 h that also shows crystal fracture.

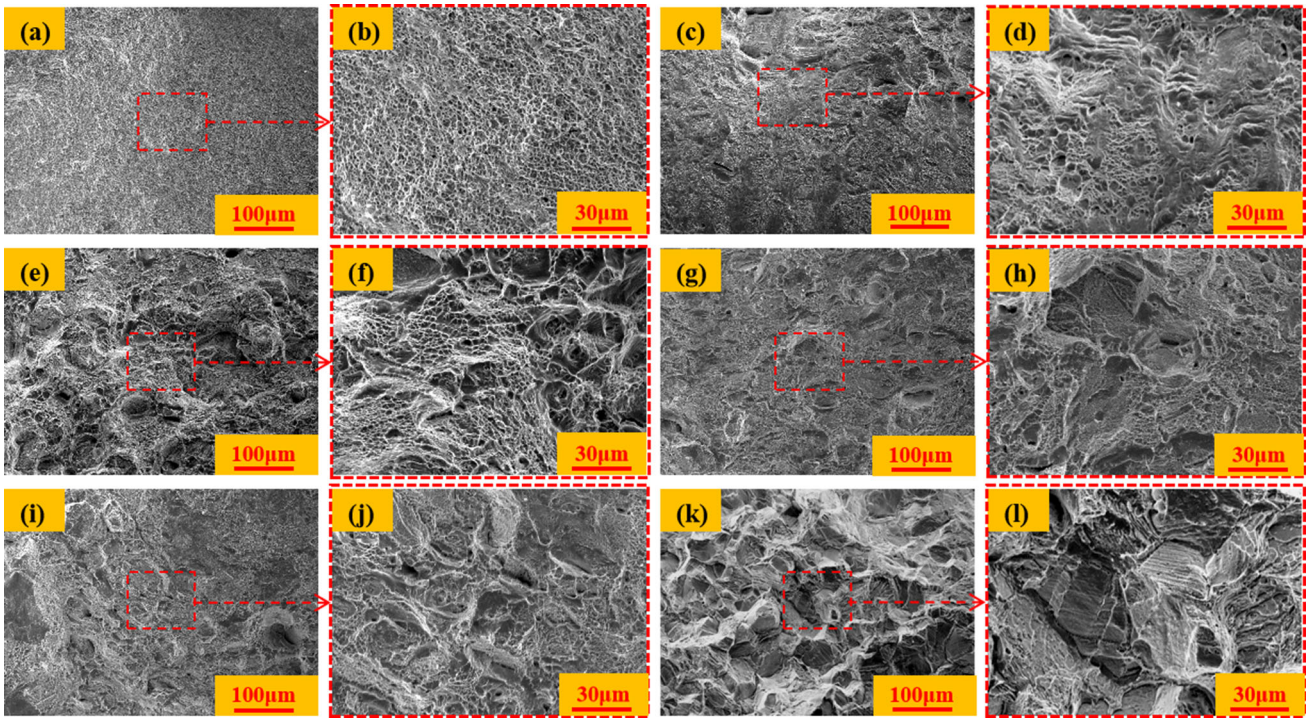

Fig. 7 Tensile fracture morphology of HEAs after different aging treatments: (a) 4 h, (c) 8 h, (e) 16 h, (g) 32 h, (i) 64 h, (k) 128 h; and (b), (d), (f), (h), (j), and (l) are the local enlarged images of the corresponding regions, respectively

Acknowledgments

The authors wish to thank the National Natural Science Foundation of China (52161011), Natural Science Foundation of Guangxi Province (2023GXNSFDA026046), Guangxi Science and Technology Project (Guike AB24010247), Central Guiding Local Science and Technology Development Fund Project (Guike ZY23055005), Scientific Research and Technology Development Program of Guilin (20220110-3), Scientific Research and Technology Development Program of Nanning Jiangnan district (20230715-02), Guangxi Key Laboratory of Superhard Material (2022-K-001), Guangxi Key Laboratory of Information Materials (231003-Z, 231033-K and 231013-Z), Engineering Research Center of Electronic Information Materials and Devices, Ministry of Education (EIMD-AB202009), the Major Research Plan of the National Natural Science Foundation of China (92166112), the Projects of MOE Key Lab of Disaster Forecast and Control in Engineering in Jinan University (20200904006), and the Open Project Program of Wuhan National Laboratory for Optoelectronics (2021WNLOKF010) for the financial support given to this work.

Data Availability

The data that support the findings of this study are available from the corresponding author upon reasonable request.

Conflict of interest

The authors declare that they have no known competing financial interests or personal relationships that could have appeared to influence the work reported in this paper.

References

1. J.W. Yeh, S.K. Chen, S.J. Lin, J.Y. Gan, T.S. Chin, T.T. Shun, C.H. Tsau, and S.Y. Chang, Nanostructured High-Entropy Alloys with Multiple Principal Elements: Novel Alloy Design Concepts and Outcomes, *Adv. Eng. Mater.*, 2004, **6**, p 299–303.
2. J.W. Yeh, Recent Progress in High-Entropy Alloys, *Ann. Chim-sci. Mat.*, 2006, **31**(6), p 633–648.
3. D.B. Miracle and O.N. Senkov, A Critical Review of High Entropy Alloys and Related Concepts, *Acta Mater.*, 2017, **122**, p 448–511.
4. H. Jiang, L. Jiang, D.X. Qiao, Y.P. Lu, T.M. Wang, Z.Q. Cao, and T.J. Li, Effect of niobium on Microstructure and Properties of the $CoCrFeNb_xNi$ high Entropy Alloys, *J. Mater. Sci. Technol.*, 2017, **33**(7), p 712–717.
5. Y. Qiu, S. Thomas, M.A. Gibson, H.L. Fraser, and N. Birbilis, Corrosion of high Entropy Alloys, *NPJ Mat. Degrad.*, 2017, **1**(1), p 299–303.
6. Y. Wei, Y. Fu, Z. Pan, Z.M. Pan, Y.C. Ma, H.X. Cheng, Q.C. Zhao, H. Luo, and X.G. Li, Influencing Factors and Mechanism of High-Temperature Oxidation of High-Entropy Alloys: A Review, *Int. J. Min. Met. Mater.*, 2021, **28**(6), p 915–930.
7. Y. Qiu, M.A. Gibson, H.L. Fraser, and N. Birbilis, Corrosion Characteristics of High Entropy Alloys, *Mater. Sci. Tech. lond.*, 2015, **31**, p 1235–1243.
8. Z.P. Lu, H. Wang, M.W. Chen, I. Baker, J.W. Yeh, C.T. Liu, and T.G. Nieh, An assessment on the Future Development of High-Entropy Alloys: Summary from a Recent Workshop, *Intermetallics*, 2015, **66**, p 67–76.
9. B.X. Cao, T. Yang, W.H. Liu, and C.T. Liu, Precipitation-Hardened High-Entropy Alloys for High-Temperature Applications: A Critical Review, *MRS Bull.*, 2019, **44**(11), p 854–859.
10. Y.S. Geng, J. Chen, H. Tan, J. Cheng, J. Yang, and W.M. Liu, Vacuum Tribological Behaviors of CoCrFeNi high Entropy Alloy at Elevated Temperatures, *Wear*, 2020, **456**, 203368
11. Y. Qi, T. Cao, H. Zong, Y. Wu, and J. Sun, Enhancement of Strength-Ductility Balance of Heavy Ti and Al Alloyed FeCoNiCr High-Entropy Alloys Via Boron Doping, *J. Mater. Sci. Technol.*, 2021, **75**(16), p 154–163.

12. S. Kumar, A. Patnaik, A.K. Pradhan, and V. Kumar, Effect of Cobalt Content on Thermal, Mechanical, and Microstructural Properties of $Al_{0.4}FeCrNiCo_x$ (x=0, 0.25, 0.5, 1.0mol) High-Entropy Alloys, *J. Mater. Eng. Perform.*, 2019, **28**, p 4111–4119.
13. X.T. Liu, W.B. Lei, L.J. Ma, J.L. Liu, J. Liu, and J.Z. Cui, Effect of Boron on the Microstructure, Phase Assemblage and Wear Properties of $Al_{0.5}CoCrCuFeNi$ High-Entropy Alloy, *Rare Metal. Mat. Eng.*, 2016, **45**(9), p 2201–2207.
14. C. Nguyen, A.K. Tieu, G. Deng, D. Wexler, B. Tran, and T.D. Vo, Study of Wear and Friction Properties of a Co-free $CrFeNiAl_{0.4}Ti_{0.2}$ High Entropy Alloy from 600 to 950 °C, *Tribol. Int.*, 2022, **169**, p 107453.
15. M.H. Xiao, J.W. Chen, J.J. Kang, K. Chen, D. Wu, and N. Gao, Effect of Heat Treatment Process on Mechanical Properties and Microstructure of $FeAlCoCrNiTi_{0.5}$ alloy, *J. Technol. Sci.*, 2018, **8**, p 095322.
16. V. Nandal, K. Hariharan, R. Sarvesha, S.S. Singh, E.W. Huang, Y.J. Chang, A.C. Yeh, S. Neelakantan, and J. Jain, Aging Temperature Role on Precipitation Hardening in a Non-Equiatomic AlCoCrFeNiTi High-Entropy Alloy, *Mater. Sci. Tech. lond.*, 2021, **37**, p 1270–1279.
17. Y. Lu, K. Zhang, B.B. Zhao, X.P. Dong, F. Sun, B.X. Zhou, Y.Q. Zhen, and L.T. Zhang, Balanced Mechanical Properties of Al03CoCrFeNiTix High-Entropy Alloys by Tailoring Ti Content and Heat Treatment, *Mat. Sci. Eng. A*, 2023, **866**, p 144677.
18. H.L. Peng, L. Hu, L.J. Li, and W.P. Zhang, Ripening of $L1_2$ Nanoparticles and their Effects on Mechanical Properties of $Ni_{28}Co_{28}Fe_{21}Cr_{15}Al_4Ti_4$ High-Entropy Alloys, *Mat. Sci. Eng. A*, 2020, **772**, 138803
19. G.W. Zhao, D. Li, G.X. Xu, D. Fang, Y.S. Ye, C.H. Huang, and Z.M. Shi, As-Cast high Entropy Shape Memory Alloys of $(TiHfX)_{50}(NiCu)_{50}$ with Large Recoverable Strain and Good Mechanical Properties, *J. Mater. Eng. Perform.*, 2022, **31**(12), p 10089–10098.
20. Y.J. Chang and A.C. Yeh, The Evolution of Microstructures and High Temperature Properties of $AlxCo_{1.5}CrFeNi_{1.5}Tiy$ High Entropy Alloys, *J. Alloy. Compd.*, 2015, **653**, p 379–385.
21. Y. Qiu, S. Thomas, D. Fabijanic, A.J. Barlow, H.L. Fraser, and N. Birbilis, Microstructural Evolution, Electrochemical and Corrosion Properties of $Al_xCoCrFeNiTi_y$ High Entropy Alloys, *Mater. Design*, 2019, **170**, 107698
22. B. Gludovatz, A. Hohenwarter, D. Catoor, E.H. Chang, E.P. George, and R.O. Ritchie, A Fracture-Resistant High-Entropy Alloy for Cryogenic Applications, *Science*, 2014, **345**, p 1153–1158.
23. L. Zhang, Y. Zhou, X. Jin, X.Y. Du, and B.S. Li, The Microstructure and High-Temperature Properties of Novel Nano Precipitation-Hardened Face Centered Cubic High-Entropy Superalloys, *Scr. Mater.*, 2018, **146**, p 226–230.
24. Y.L. Zhao, T. Yang, Y.R. Li, L. Fan, B. Han, Z.B. Jiao, D. Chen, C.T. Liu, and J.J. Kai, Superior High-Temperature Properties and Deformation-Induced Planar Faults in a Novel $L1_2$-Strengthened High-Entropy Alloy, *Acta Mater.*, 2020, **188**, p 517–527.
25. A. Kumar, A.K. Swarnakar, and M. Chopkar, Phase Evolution and Mechanical Properties of $AlCoCrFeNiSi_x$ High-Entropy Alloys Synthesized by Mechanical Alloying and Spark Plasma Sintering, *J. Mater. Eng. Perform.*, 2018, **27**(7), p 3304–3314.
26. N. Diomidis and S. Mischler, Third Body Effects on Friction and Wear during Fretting of Steel Contacts, *Tribol. Int.*, 2011, **44**(11), p 1452–1460.
27. J. Joseph, N. Haghdadi, K. Shamlaye, P. Hodgson, M. Barnett, and D. Fabijanic, The Sliding Wear Behaviour of CoCrFeMnNi and $Al_xCoCrFeNi$ High Entropy Alloys at Elevated Temperatures, *Wear*, 2019, **428**, p 32–44.
28. Y. Yu, F. He, Z.H. Qiao, Z.J. Wang, W.M. Liu, and J. Yang, Effects of Temperature and Microstructure on the Triblogical Properties of $CoCrFeNiNb_x$ Eutectic High Entropy Alloys, *J. Alloy. Compd.*, 2019, **775**, p 1376–1385.
29. B. Cao, T. Yang, W.H. Liu et al., Precipitation-Hardened High-Entropy Alloys for High-Temperature Applications: A Critical Review, *MRS Bull.*, 2019, **44**(11), p 854–859.
30. W. He, C. Zeng, W. Yang et al., Impact of Different Cr Contents on Microstructural Evolution and Mechanical Behaviour of $CoCr_xCuFeMnNiV$ High-Entropy Alloys, *J. Mater. Res. Technol.*, 2022, **21**, p 4577–4590.
31. Y.W. Wu, X.Y. Zhao, Q. Chen, C. Yang, M.G. Jiang, C.Y. Liu, Z. Jia, Z.W. Chen, T. Yang, and Z.Y. Liu, Strengthening and Fracture Mechanisms of a Precipitation Hardening High-Entropy Alloy Fabricated by Selective Laser Melting, *Virtual Phys. Prototy.*, 2022, **17**(3), p 451–467.
32. S.Y. Li, F.D. Chen, X.B. Tang, G.J. Ge, Z.J. Sun, Z.L. Geng, M.Y. Fan, and P. Huang, Effect of Ti on the Microstructure and Mechanical Properties of $AlCrFeNiTi_x$ Eutectic High-Entropy Alloys, *J. Mater. Eng. Perform.*, 2022, **31**(10), p 8294–8303.
33. H. Wu, S.R. Huang, C.Y. Zhu, H.G. Zhu, and Z.H. Xie, Influence of Cr content on the microstructure and mechanical properties of $Cr_xFeNiCu$ high entropy alloys, *Prog. Nat. Sci.*, 2020, **30**(2), p 239–245.
34. S. Dasari, Y.J. Chang, A. Jagetia et al., Discontinuous Precipitation Leading to Nano-Rod Intermetallic Precipitates in an $Al_{0.2}Ti_{0.3}Co_{1.5}CrFeNi_{1.5}$ High Entropy Alloy Results in an Excellent Strength-Ductility Combination, *Mat. Sci. Eng. A*, 2021, **805**, p 140551.
35. Y. Tong, D. Chen, B. Han et al., Outstanding Tensile Properties of a Precipitation-Strengthened $FeCoNiCrTi_{0.2}$ High-Entropy Alloy at Room and Cryogenic Temperatures, *Acta Mater.*, 2019, **165**, p 228–240.
36. J.Y. Zhang, C.C. Zhao, Y.J. Wu et al., Structural Characteristic and Crystallization Behavior of the $(Fe_{0.33}Co_{0.33}Ni_{0.33})_{84-x}Cr_8Mn_8Bx$ High-Entropy-Amorphous Alloy Ribbons, *Acta Metall. Sin.*, 2022, **58**(2), p 215–224.